# BASAL DISLOCATION MOBILITY IN ZINC SINGLE CRYSTALS

K. H. Adams*, T. Vreeland, Jr., and D. S. Wood
W. M. Keck Laboratory of Engineering Materials
California Institute of Technology
Pasadena, California

ABSTRACT

Experimental measurements of basal dislocation mobility and the strain-rate sensitivity of the flow stress have been made on 99.999% pure zinc single crystals. Dislocation mobility in the $[\bar{1}2\bar{1}0]$ (0001) basal slip system was measured by observing slip band growth produced by load pulses of controlled amplitude and duration. Local rearrangement of dislocations occurs at a resolved stress of 7 $lb/in^2$. Slip bands are formed at stresses greater than 7 $lb/in^2$, and their growth velocities are in the range of 7 to 80 cm/sec for shear stresses between 7 and 12 $lb/in^2$. The results of the experimental measurements of dislocation mobility are discussed in relation to current theories. A comparison of the strain-rate sensitivity and the mobility measurements shows that a significant change in the density of moving dislocations is associated with a change in strain-rate. This change in density has generally been ignored by previous investigators. A dislocation model is proposed to explain the observed strain-rate sensitivity.

## Introduction

The stress dependence of the mobility of dislocations has been clearly established for a variety of b.c.c. metal, ionic and semiconducting crystals by various investigators. Etch pit methods have been used to establish the mobility relation for 3.25% silicon-iron [1], tungsten [2], LiF [3], NaCl [4], Si [5], and Ge [5, 6]. No direct determinations of dislocation mobility in bulk size crystals of f.c.c. or h.c.p. metals have been reported. A basic understanding

---

* Present Address: Department of Mechanical Engineering, Tulane University, New Orleans, Louisiana.

of the dynamic stress-strain behavior of f.c.c. and h.c.p. metals will be achieved when dislocation mobility studies have been conducted on these classes of metals.

The direct determination of dislocation velocity by etch pit techniques is very tedious and requires a reliable etching technique for revealing dislocations in every material of interest. Since reliable techniques are not available for many materials, there is a great need for indirect experiments which can be used to deduce the stress dependence of the dislocation mobility. Guard (7) has suggested a method for determining the stress dependence of the dislocation mobility by an indirect test. The plastic strain-rate, $\dot{\gamma}_p$, of a crystalline solid is a function of the density of moving dislocations $\rho_m$, the Burgers vector of the dislocations, b, and the average dislocation velocity, v, through the relation

$$\dot{\gamma}_\rho = \rho_m b v \qquad (1)$$

Therefore, the power dependence of the dislocation velocity is related to the strain-rate sensitivity of the flow stress, $\partial \ln \tau / \partial \ln \dot{\gamma}_p$, by the relation

$$\frac{\partial \ln \dot{\gamma}_p}{\partial \ln \tau} = \frac{\partial \ln \rho_m}{\partial \ln \tau} + \frac{\partial \ln v}{\partial \ln \tau} \qquad (2)$$

where the power dependence of the dislocation velocity or mobility exponent is equal to $\partial \ln v / \partial \ln \tau$. The inverse strain-rate sensitivity will be equal to the mobility exponent if $\partial \ln \rho_m / \partial \ln \tau$ is zero. Johnston and Stein (8) have shown this to be the case for LiF and 3.25% silicon-iron if the inverse strain-rate sensitivity is extrapolated to zero strain. Schadler (2) has shown this extrapolation procedure to be inaccurate for tungsten. The validity of this method as applied to other materials has not as yet been established.

This paper describes the results of the direct determination of basal dislocation mobility by etch pit methods and the relation between the mobility exponent and the inverse strain-rate sensitivity in zinc single crystals.

## Experimental Procedure

### Specimen preparation

Single crystals were prepared from C.P. grade zinc of 99.999% purity obtained from the New Jersey Zinc Company. An analysis of this material furnished by the supplier indicated the following impurities in wt. %: Pb = 0.0002; Fe = 0.0002; Cd = 0.00005; other < 0.00011. Single crystals were grown by a modified Bridgeman technique in graphite coated Pyrex molds. Cylindrical single crystals 7/8 in. in diameter and 8 in. long were grown.

The 7/8 in. diameter crystals were acid sawed into sections using 8N $HNO_3$ on a stainless steel wire. The crystallographic orientation of each section was found by observation of the orientation and markings on a cleavage surface of the crystal. Cleaving was done in liquid nitrogen with a needle struck by a light hammer. The cleavage surface established the (0001) basal plane and cleavage steps, which were found to correspond to twinning traces, were used to establish the $[\bar{1}2\bar{1}0]$ direction in the (0001) plane. These cleavage steps were probably formed by basal cleavage within twinned material.

Test specimens in the form of 1/2 in. cubes were machined from acid sawed and cleaved sections with the use of a Servomet Electric Spark Discharge Machine. The spark machining consisted of trepanning and planing operations at minimum spark energy settings. All spark machining operations were done in oil at 200° - 210° F to prevent cleavage cracks. The damage produced by spark discharge machining and the methods used to reduce such damage have been described by Turner et al (9).

Test specimens with two different orientations of the basal slip plane with respect to the load axis were used. Figure 1 shows the two orientations of the specimens, all of which have a set of $(10\bar{1}0)$ prism surfaces. The $(10\bar{1}0)$ surfaces were used to reveal basal dislocations by the etching technique of Brandt et al (10).

The machining operations resulted in specimen surfaces which were parallel to within 0.1°. The surface finish achieved by spark planing was of the order of 10 $\mu$ in r.m.s. The manner in which the test specimens were machined resulted in some uncertainty in the orientation of the basal slip system with respect to the specimen surfaces on which compressive forces were applied during subsequent testing. This crystallographic uncertainty was sufficiently small to produce a maximum uncertainty in basal resolved shear stress of ± 1%.

Damage to the specimens resulting from the spark machining operations was removed chemically by polishing off approximately 0.005 in. of material and annealing at 700° F in a purified hydrogen atmosphere for 4 to 8 hours. The loading surfaces were masked with tape during the polishing to retain a flat surface.

Velocity measurements

A standard method for determining dislocation mobility by etch pit techniques has been used by many investigators (1, 2, 3, 4, 5, 6). Generally the method involves scratching a well annealed crystal to introduced fresh unpinned dislocations in a known region in the vicinity of the scratch. A stress pulse of known amplitude and duration is then applied. The specimen is re-etched to


(a) 45° Specimen


(b) 80° Specimen

FIG. 1

Crystallographic Orientation of Test Specimens.

determine the final location of the dislocations in the scratched region and a dislocation velocity is computed from the measured dislocation displacement and time duration of the pulse test. The successful use of this standard method usually requires that only dislocations induced by the scratch move during the application of the load and that dislocation displacements produced are small compared to the average distance between grown-in dislocations so that the fresh dislocations can be differentiated from the background dislocation density.

The standard method was used in the present investigation with some minor variations and additions. In most cases, however, pulse tests were conducted without the introduction of fresh dislocations prior to the test. The reason for this will be discussed subsequently.

Each specimen was etched prior to a pulse test and after the introduction of intentional damage, if any, and replicas were made of the etched surfaces to record the initial dislocation density and configuration on $(10\bar{1}0)$ prism surfaces of the specimen. Replicas were made using a replication solution obtained from Ladd Industries and 0.005 in. thick cellulose acetate film. The transparent replicas were subsequently coated with a vapor deposited layer of aluminum at vacuum pressures of less than $5 \times 10^{-5}$ mm of Hg. An optically opaque film of aluminum was sufficiently reflective for optical examination with a metallurgical microscope and was not so thick as to obscure details on the replicas at magnifications less than 500X.

Figure 2 illustrates the damage produced on a $(10\bar{1}0)$ prism surface by two scratches with a diamond phonograph stylus with a contact load of 1.25g.

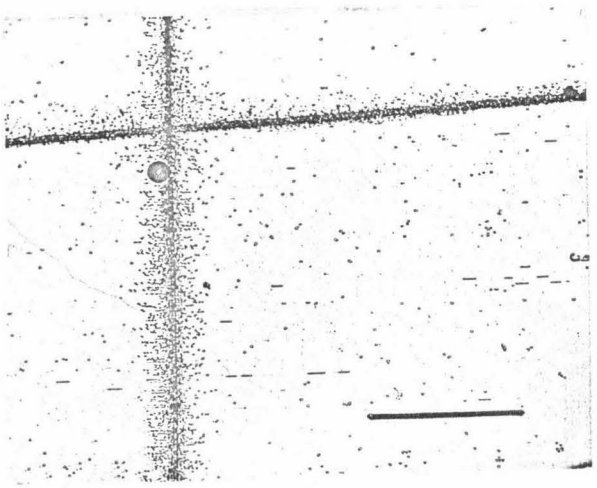

FIG. 2
Prism surface of test specimen prior to pulse testing shown damage produced by two scratches. Line indicates $[\bar{1}2\bar{1}0]$ direction Magnification X100.

Fig. 2 is a photomicrograph of a replica taken prior to testing. The background density of dislocations in Fig. 2 is generally representative of the density found in all the as-grown, annealed specimens used in this investigation.

After pulse testing, the specimens were re-etched and again replicated. The elapsed time between test and re-etch was usually limited to less than 3 min to minimize dislocation rearrangement. Mercury introduced during the initial etch was sufficient to cause etch pits to form during the second etch (10). The number of pulse tests that could be conducted before the specimen had to be annealed was determined by the amount of deformation or increase in dislocation density produced in a series of tests and by the conditions of the $(10\bar{1}0)$ specimen surfaces after several re-etching operations. In several cases, as many as twenty pulse tests were conducted on a specimen before high temperature annealing was required because the dislocation density had reached too high a level.

Before annealing specimens which had been previously etched, a vacuum treatment was required to remove the mercury from the surfaces. Specimens were placed in a vacuum of $10^{-6}$ to $10^{-5}$ mm of Hg for 8 h for this purpose. Subsequent annealing was carried out in a purified hydrogen atmosphere at 700° F for 4 to 8 h. This annealing procedure was also used after each strain-rate sensitivity test to return the specimen to as near its original pretest condition as possible.

The pulse load tests were carried out using a special compression test fixture in the rapid load tensile testing machine of Russell et al (11). The testing equipment was capable of applying constant amplitude load pulses with a rise time of 2 msec and a minimum duration of 17 msec. Records of load vs time were obtained with a Consolidated Electrodynamics oscillograph using a four leg dynamometer bridge of high output silicon filament strain gages obtained from Micro-systems, Inc. An example of a typical load pulse is given in Fig. 3.

The compression fixture used in connection with a rapid load machine, as shown schematically in Fig. 4, as a self-aligning system of spherical seats supported by air pressure. The air bearing feature minimizes alignment errors due to friction between the bearing surfaces and hence reduces the error produced when the load axis is off the centroid of the specimen. In addition, a sheet of 0.001 in. teflon was used between the loading surfaces of the specimen and the spherical seats to reduce friction and the effect of surface irregularities. The combined uncertainty in basal resolved shear stress caused by crystallographic orientation uncertainty, specimen alignment error and errors resulting

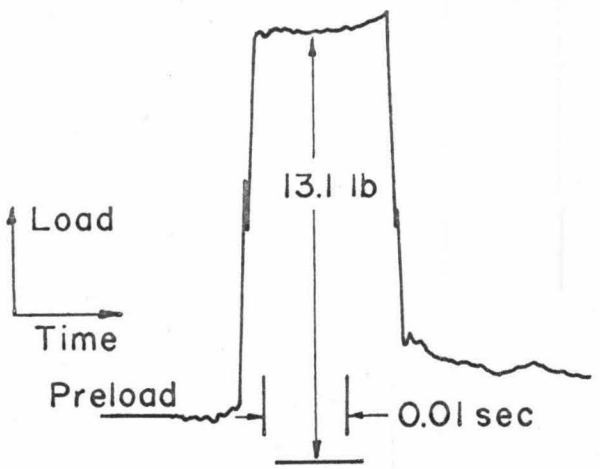


FIG. 3
Tracing of a Typical Pulse Load Record

from friction in the load bearings was estimated to be less than 5%.

Strain-rate sensitivity

The method used in this investigation for determining the strain-rate sensitivity of the flow stress for basal slip was to determine the incremental change in flow stress caused by a rapid change in strain-rate. Tests were conducted on specimens in which the basal slip system was oriented at 45° to the compression axis as shown in Fig. 1.

Compression tests were performed in an Instron testing machine and compressive strain resulting from basal shear was measured with a parallel plate capacitor system connected to a Robertshaw proximity meter. Figure 5 is a schematic drawing of the compression fixture showing the relation between the parallel plate capacitor and the test specimen. The output of the proximity meter and the Instron load cell was recorded vs time on a Consolidated Electrodynamics oscillograph. A load sensitivity of 10 lb/7 in. of oscillograph paper was maintained throughout each test. The total sensitivity of the strain measuring system was governed by the initial plate spacing, the plate area of the capacitance gage and the sensitivity scale of the proximity meter. The initial plate spacing used was 0.1 in. which together with a plate area of 5 $in.^2$ resulted in a full scale output corresponding to 0.0004 in. change in plate spacing on the maximum sensitivity range of the proximity meter. The maximum sensitivity range

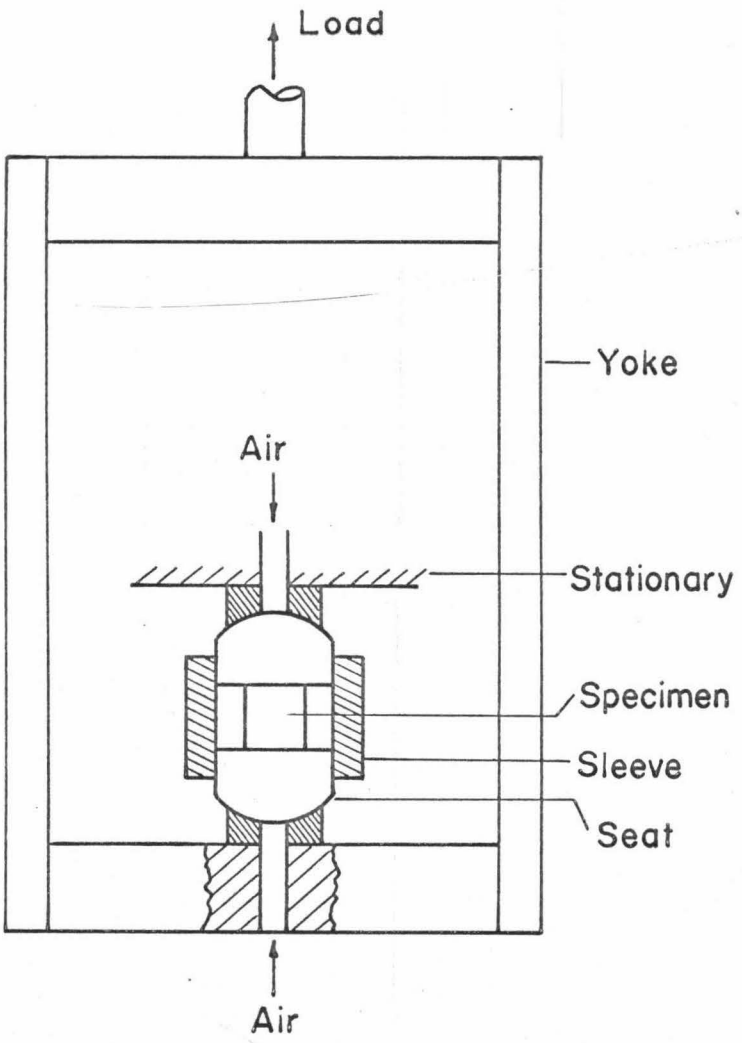


FIG. 4

Schematic of Compression Fixture For Rapid Load Machine

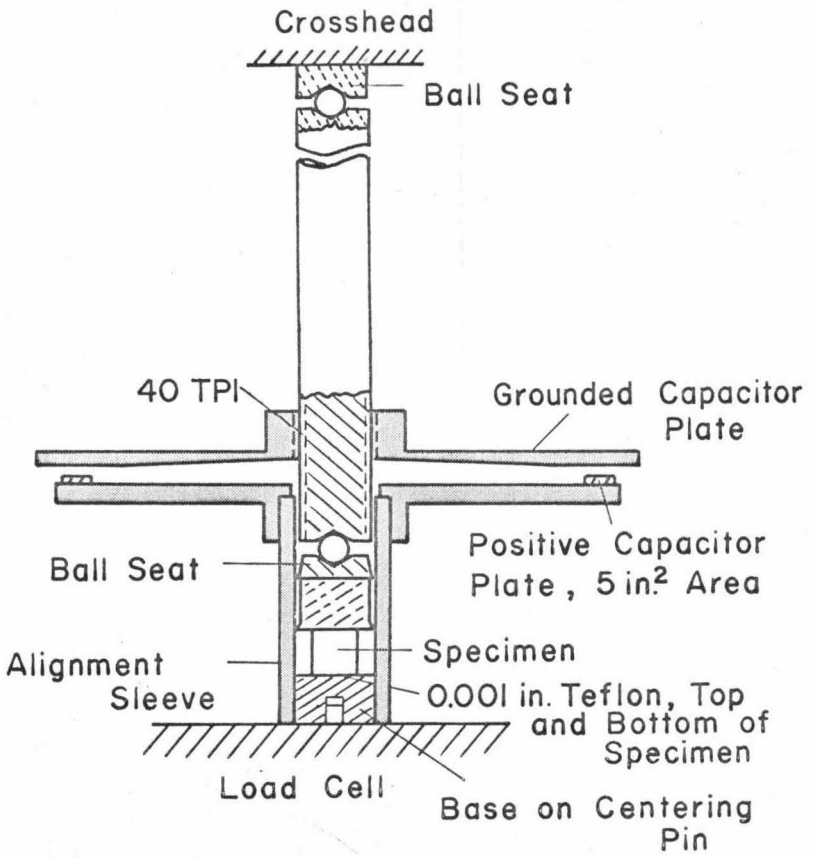


FIG. 5

Schematic of Test Fixture For Strain-Rate Sensitivity Tests

was not maintained throughout a test.

Strain-rate changes were made during the tests by changing the crosshead speed of the Instron in the ratio 1/ $\frac{1}{3}$ / $\frac{1}{10}$ / 0. Full speed corresponded to the synchronous crosshead speed of the Instron and this speed varied between 0.001 in./min and 0.005 in./min depending on the final value of strain of a test. Figure 6 is a tracing of the oscillograph record obtained with a complete sequence of crosshead speed changes. Load changes corresponding to strain-rate changes were measured for both increasing and decreasing changes in crosshead speed.

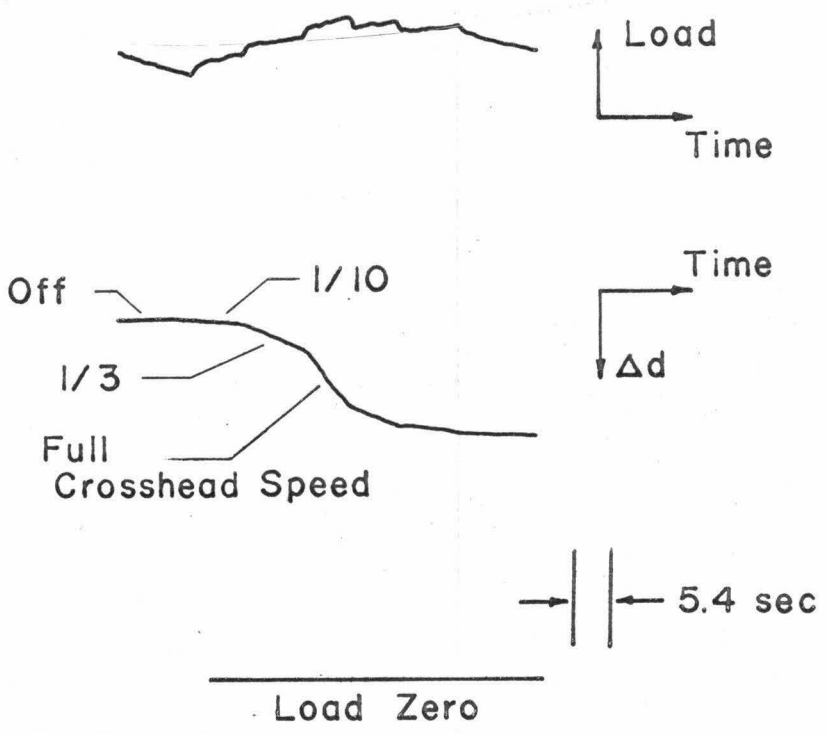


FIG. 6
Tracing of Oscillograph Record

The load relaxation which occurs when the crosshead is stopped is due primarily to a characteristic of the machine as demonstrated by using a brass specimen which exhibits only elastic strain at the test loads. The capacitance gage readings due to elastic strain in the fixture were determined using a brass specimen in place of a zinc crystal specimen. The elastic compliance of the fixture was calculated from the measured capacitance gage readings and the loads

applied to the brass specimen. The measured elastic compliance and the compliance of the load cell were used to estimate the errors involved in assuming the crosshead speed ratios were equal to the corresponding plastic strain-rate ratios in tests on zinc single crystals. This was a more accurate means of estimating the errors than measuring strain-rates directly because the load sensitivity of the system was relatively much greater than the strain sensitivity. The relation between the compressive plastic strain-rate ratio, $\dot{\varepsilon}_{p_1} / \dot{\varepsilon}_{p2}$, and the crosshead speeds, $\dot{y}$, is given by

$$\frac{\dot{\varepsilon}_{p_1}}{\dot{\varepsilon}_{p2}} = \frac{\dot{y}_1 - C_T \dot{L}_1}{\dot{y}_2 - C_T \dot{L}_2}$$

where $\dot{L}$ is the load rate and $C_T$ is the total elastic compliance of the system including both ball seats, the load cell and the specimen. For basal strain-rate tests, the maximum error in assuming

$$\frac{\dot{\varepsilon}_{p_1}}{\dot{\varepsilon}_{p_2}} = \frac{\dot{y}_1}{\dot{y}_2}$$

was found to be less than 5%, so no correction for elastic strain of the system was made in the analysis of the records.

## Experimental Results

### Velocity measurements

Pulse tests performed at resolved shear stresses up to 19 lb/in.$^2$ and for durations of from 17 msec to 1 sec gave information from which the basal dislocation mobility is deduced. The following general observations were made in these tests:

(1) Stress pulses of amplitude less than 7 lb/in.$^2$ produced no increase in dislocation density, but some local rearrangement of dislocations was occasionally observed.

(2) Stress pulses of amplitude greater than 7 lb/in.$^2$ produced an increase in dislocation density and in particular, the formation of pile-ups was observed near sub-boundaries. Dislocation sources within the specimen or at the surfaces where the load was applied appeared to operate and cause dislocation pile-ups at the same stress levels that influenced the fresh dislocations produced by scratches. This, in effect, prevented any one-to-one correspondence of before and after dislocation positions from being made. Long, extended pile-ups along basal slip plane traces were observed within the shear stress range of 7 to 19 lb/in.$^2$ Often the length of an individual pile-up against a

sub-boundary was much less than the spacing of sub-boundaries, but pile-ups on adjacent sub-boundaries appeared in the same slip plane trace. These pile-ups generally extended to at least one specimen edge and could often be traced across the entire specimen. In several tests, dislocation pile-ups, which appeared to lie on a single plane, were observed on opposite $(10\bar{1}0)$ surfaces of the test specimen. This indicates that dislocations moved a distance equal to the width of the specimen ($\frac{1}{2}$ in.) in the direction normal to the slip vector during the period of the load pulse.

Typical areas showing the dislocation structure before a load pulse, and the pile-ups observed after a load pulse, are shown in Fig. 7 and 8. The long pile-ups in Fig. 7 extend across the entire specimen.

(3) The number of pile-ups, and the density of dislocations increase as the stress pulse amplitude is increased.

(4) Break-up of some of the substructure is observed at stresses above approximately 15 lb/in.$^2$ which is the macroscopic yield strength of 99.999% zinc single crystals (12) (see Fig. 7).

The distance along the slip plane from the edge of the specimen to the furthest sub-boundary which exhibited a pile-up was assumed to be the distance traversed by the leading dislocation in the pile-up. The velocity of the leading dislocation was taken to be the distance moved divided by the pulse duration. The results of a series of pulse tests are presented in Table I where $\tau$ is the resolved shear stress and v is dislocation velocity. Log velocity has been plotted vs log resolved shear stress in Fig. 9. Points labelled with a caret ($\wedge$) are measurements on pile-up lengths that extended across the entire specimen face and hence are to be regarded as lower limits for the velocity at the corresponding stress level. The points in Fig. 9 without a caret represent pile-up lengths that extended from a load surface into the specimen. Each point represents the maximum velocity calculated for a given test and hence involves the maximum length of all the observed dislocation pile-ups.

Figure 9 shows a considerable scatter in the experimental data. A straight line has been drawn through the points representing the maximum observed velocity for a given stress level. The straight line indicates that the date can be represented by an empirical power function relation of the form:

$$v = \left(\frac{\tau}{\tau_o}\right)^n \tag{3}$$

where $\tau$ is the applied shear stress, n = 5 and $\tau_o$ equals the shear stress corresponding to a velocity of 1 cm/sec and is 5 lb/in.$^2$. Several sources of error existed that may explain the scatter observed. One of the uncertainties

TABLE I

Dislocation Velocity Data

| Specimen No. | Test No. | $\tau$ (lb/in.$^2$) | v (cm/sec) | $\tau - \tau_i$ $\tau_i$ = 6 lb/in.$^2$ |
|---|---|---|---|---|
| 18-1 | 6 | 7.1 | 6.6 | 1.1 |
| 18-6 | 4 | 7.2 | 6.9 | 1.2 |
| 18-1 | 7 | 7.6 | 6.0 | 1.6 |
| 18-6 | 6 | 8.3 | 13.4 | 2.3 |
| 18-6 | 7 | 8.8 | 6.7 | 2.8 |
| 18-1 | 8 | 8.9 | 3.6 | 2.9 |
| 18-3 | 1 | 9.0 | 5.0 | 3.0 |
| 18-3 | 2 | 9.2 | 9.1 | 3.2 |
| 18-6 | 8 | 9.4 | 13.4 | 3.4 |
| 18-3 | 3 | 9.9 | 9.1 | 3.9 |
| 18-1 | 9 | 10.0 | 26.6* | 4.0 |
| 18-1 | 11 | 10.9 | 42.3* | 4.9 |
| 18-3 | 6 | 11.2 | 18.4 | 5.2 |
| 18-1 | 14 | 11.6 | 14.4 | 5.6 |
| 18-1 | 12 | 11.8 | 75.3* | 5.8 |
| 18-6 | 1 | 11.9 | 25.0* | 5.9 |
| 18-1 | 15 | 12.1 | 75.3* | 6.1 |
| 18-5 | 1 | 12.2 | 75.0* | 6.2 |
| 18-1 | 17 | 14.0 | 59.0 | 8.0 |
| 18-1 | 18 | 15.5 | 73.0* | 9.5 |
| 18-1 | 19 | 16.8 | 75.3* | 10.8 |
| 18-1 | 20 | 17.2 | 75.3* | 11.2 |
| 18-1 | 4 | 18.1 | 58.0 | 12.1 |
| 18-1 | 5 | 18.9 | 77.2* | 12.9 |

* Dislocation pile-up entirely across specimen. Other velocities involve one edge of the specimen.

(a) Before Pulse

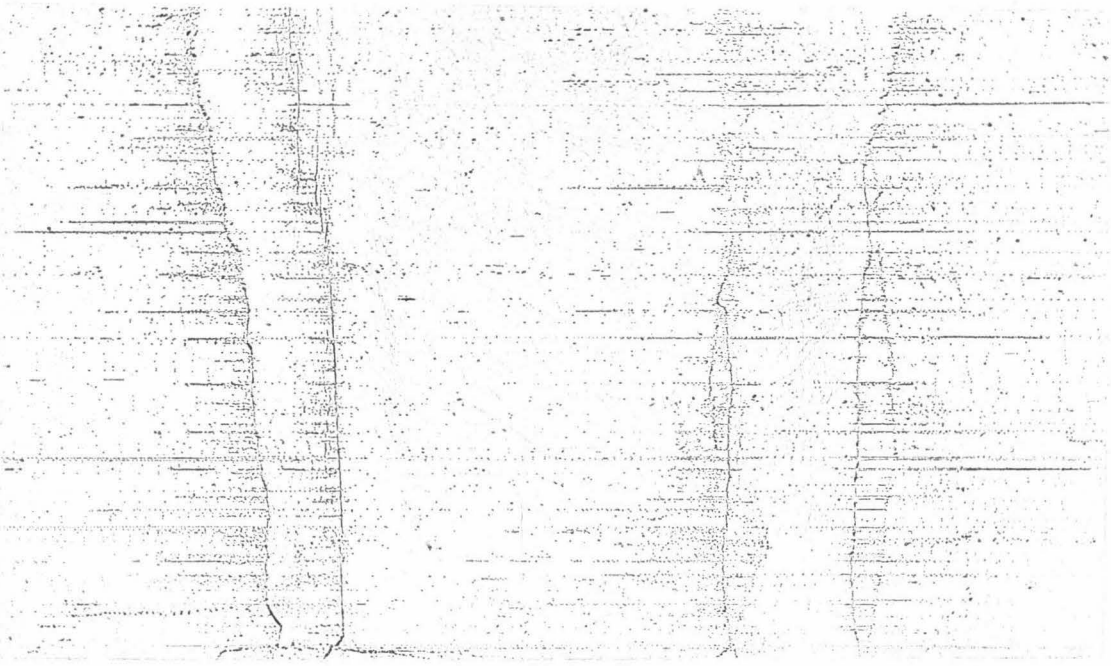

FIG. 7

Basal Dislocations Before and After a Pulse of 15.4 lb/in.$^2$, 45 sec Pulse Duration, Specimen 16-2T2 99.999 per cent Zn, 100X

(a) Before Pulse

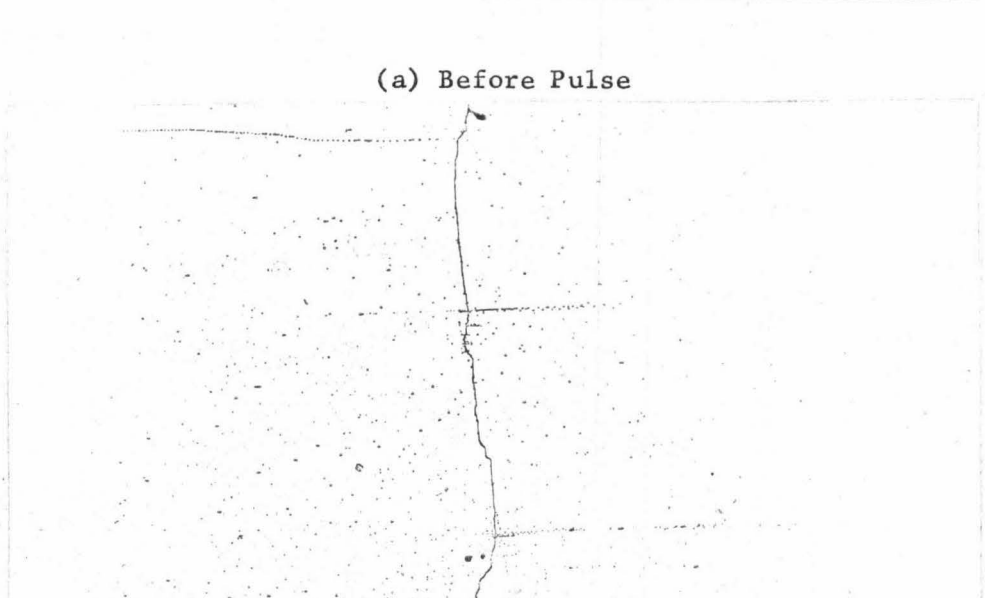

(b) After Pulse

FIG. 8

Basal Dislocations Before and After a Pulse of
12.2 lb/in.$^2$, 17 x $10^{-3}$ sec Pulse Duration, Specimen 18-5T1
99.999 per cent Zn, 100X

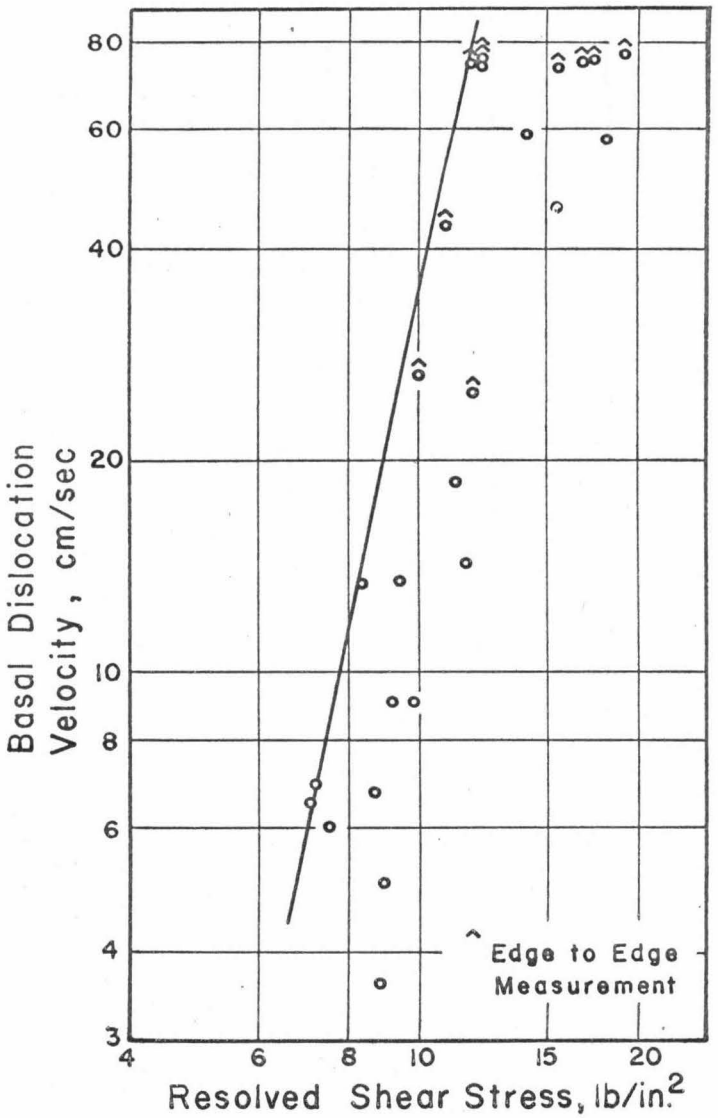


FIG. 9

Basal Dislocation Velocity vs Resolved Shear Stress

was the location of the source of the dislocation pile-up and another was introduced in the process of measuring the pile-up lengths because the location of the end point of a pile-up was not always clear.

The same data plotted in Fig. 9 is shown plotted as log velocity against $\tau - \tau_i$ in Fig. 10. A value of 6 lb/in.$^2$ was taken for $\tau_i$ which is the lowest

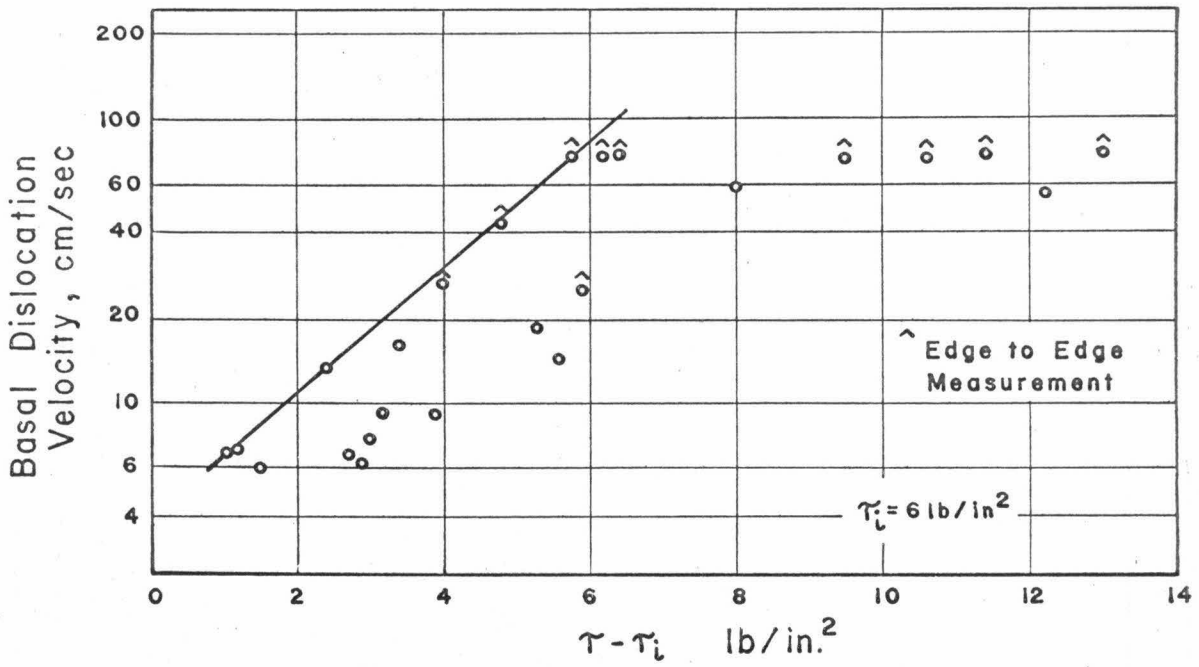


FIG. 10

Basal Dislocation Velocity vs $\tau - \tau_i$

stress at which any dislocation motion was observed. A straight line has been drawn through the maximum velocity points which represents a function of the form:

$$v = Ce^{\frac{\tau-\tau_i}{B}} \qquad (4)$$

where C is a constant and B = 1.45 lb/in.$^2$.

Strain-rate sensitivity

Two different functional relationships between the plastic strain-rate, $\dot{\gamma}_p$, and the applied shear stress were employed in analyzing the strain-rate sensitivity data. The first relation assumes a power law dependence of the

form:

$$\dot{\gamma}_p = C\,\tau^{n'} \tag{5}$$

where C is a constant. The inverse strain-rate sensitivity from Eq. 5 is given by

$$n' = \frac{\partial \ln \dot{\gamma}_p}{\partial \ln \tau}$$

or

$$n' \simeq \frac{\ln \dot{\gamma}_{p_2} / \dot{\gamma}_{p_1}}{\Delta \tau / \tau} \tag{6}$$

in terms of the strain-rate after the change, $\dot{\gamma}_{p_2}$, and that imposed prior to the change, $\dot{\gamma}_{p_1}$. $\Delta\tau$ is the jump in stress accompanying the change and is much less than the shear stress, $\tau$. The values for n' calculated from the experimental data of one test are given in Table II. A consistent variation of n' with strain was not found. The mean value for n' and the standard deviation from the mean are listed in Table III for two tests. No significant difference was found between the values of n' calculated from increasing changes and decreasing changes in strain-rate.

The second relation used in analyzing the strain-rate sensitivity data assumes that the strain-rate is related to the difference between the applied stress and the flow stress at zero strain-rate, $\tau_f$, or

$$\dot{\gamma}_p = C\,(\tau - \tau_f)^{m'} . \tag{7}$$

The exponent m' is then given as

$$m' = \frac{\partial \ln \dot{\gamma}_p}{\partial \ln (\tau - \tau_f)}$$

or

$$m' = \frac{\ln \dot{\gamma}_{p_2} / \dot{\gamma}_{p_1}}{\ln \dfrac{\tau_2 - \tau_f}{\tau_1 - \tau_f}} \tag{8}$$

where $\tau_2$ is the stress immediately after the strain-rate change and $\tau_1$ is the stress immediately prior to the strain-rate change. Measurements of the load immediately before the "machine on" part and after the "machine off" part of the strain-rate cycles were used to determine the values of $\tau_f$ for a given set of strain-rate changes. Figure 11 shows schematically a typical load-time curve obtained experimentally. The load jumps resulting from increasing

TABLE II

Strain-Rate Sensitivity Data, Specimen 16-4, Test 2.
Max Crosshead Speed 1 x $10^{-3}$ in./min

| $\tau$ (lb/in.$^2$) | $\gamma_p$ (%) | n' | m' |
|---|---|---|---|
| 14.2 | 0.01 | 77 | |
| 14.4 | 0.015 | 65 | |
| 14.5 | 0.02 | 47 | |
| 15.4 | 0.08 | 47 | 2.15 |
| 15.6 | 0.10 | 76 | |
| 15.9 | 0.12 | 90 | |
| 16.0 | 0.13 | 62 | |
| 16.2 | 0.14 | 49 | 2.97 |
| 16.4 | 0.15 | 99 | |
| 16.5 | 0.17 | 76 | |
| 17.2 | 0.24 | 62 | 1.98 |
| 17.4 | 0.25 | 105 | 1.87 |
| 17.4 | 0.25 | 79 | |
| 17.7 | 0.28 | 64 | |
| 18.6 | 0.36 | 92 | |
| 18.7 | 0.38 | 57 | 1.31 |
| 18.8 | 0.39 | 77 | |
| 18.9 | 0.41 | 95 | |
| 19.6 | 0.50 | 82 | |
| 19.8 | 0.52 | 77 | 1.92 |
| 20.0 | 0.55 | 97 | |
| 20.0 | 0.56 | 100 | |
| 20.6 | 0.63 | 86 | |
| 20.7 | 0.65 | 94 | 1.94 |
| 21.0 | 0.68 | 75 | |
| 21.4 | 0.74 | 90 | |
| 21.6 | 0.77 | 65 | 1.31 |
| 21.7 | 0.78 | 84 | |
| 21.8 | 0.80 | 78 | |
| 22.6 | 0.91 | 47 | 1.45 |
| 22.9 | 0.94 | 113 | 2.32 |
| 23.0 | 0.95 | 62 | |
| 23.5 | 1.02 | 78 | |
| 23.6 | 1.03 | 72 | 1.81 |

TABLE III

Summary of Strain-Rate Sensitivity Data, Specimen No. 16 - 4

| Test No. | Max Crosshead Speed ($10^{-3}$ in./min) | Final Strain (%) | n' | m' |
|---|---|---|---|---|
| 2 | 1 | 1.03 | 77 ± 17 | 1.91 ± 0.46 |
| 3 | 5 | 6.3 | 90 ± 20 | 2.04 ± 0.30 |

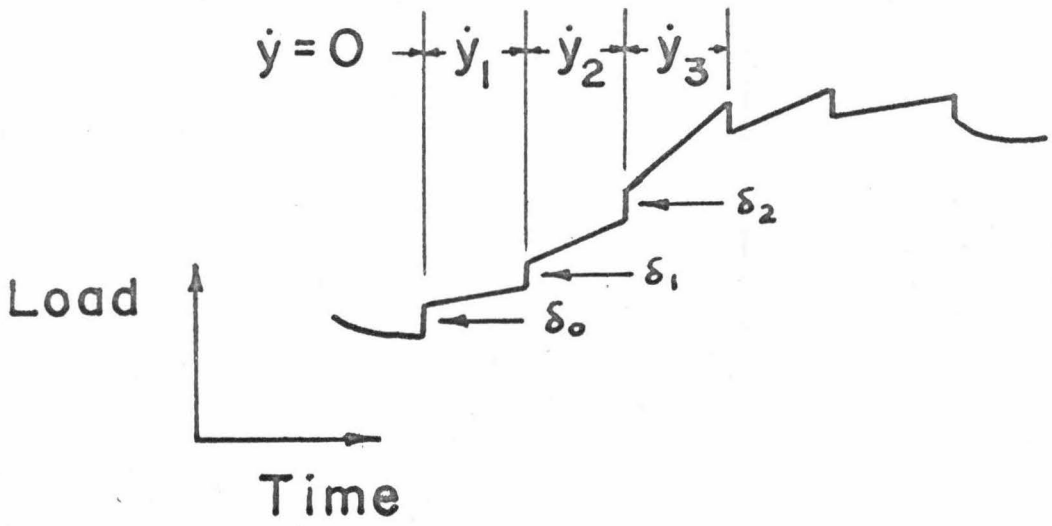


FIG. 11

Schematic of Load vs Time Curve

changes in crosshead speed, $\dot{y}$ , are shown as $\delta_o$, $\delta_1$, and $\delta_2$. The stress difference ratios are then given as

$$\frac{\tau_2 - \tau_f}{\tau_1 - \tau_f} = \frac{\delta_o + \delta_1}{\delta_o}$$

and

$$\frac{\tau_3 - \tau_f}{\tau_2 - \tau_f} = \frac{\delta_o + \delta_1 + \delta_2}{\delta_o + \delta_1} .$$

The values of m' calculated from the experimental data are given in Table II. Table III gives mean values and standard deviations from the mean for two tests. A consistent variation of m' with strain was not found.

## Discussion

### Dislocation pile-ups

The great majority of the etch pits which were produced during the pulse loading tests must have been associated with basal dislocations of predominately edge character in view of the following considerations. The specimens

were oriented such that the resolved shear stress on dislocations whose Burgers vector is parallel to the etched surface is twice as great as the resolved shear stress on dislocations with the other possible $\langle \bar{1}2\bar{1}0 \rangle$ Burgers vectors. Edge dislocations with the largest resolved shear stress therefore make a perpendicular intersection with the etch surface. Most of the dislocations lines which terminate at etch pits must be nearly perpendicular to the etch surface, and they are thus predominantly of edge orientation.

The results of the pulse tests indicate that basal dislocations moved long distances and, in some cases, out of the specimen at stress levels near the macroscopic flow stress as determined by stress-strain tests. Each dislocation pile-up against a sub-boundary appears as a single, narrow slip band. These individual pile-ups appear to be associated with other pile-ups on the same slip band. These observations imply that one very active dislocation source was responsible for an entire slip line involving hundreds of individual dislocations. Dislocation multiplication of this type would be characteristic of a Frank-Read source located at the surface or within the crystal. In almost all cases the pile-ups were observed to extend from a loaded surface of the specimen which indicates that surface sources are probably more important than volume sources. This may be due to stress concentrations on the surface where the load is applied. In addition, surface sources of a given length are able to generate dislocations at half the stress level of volume sources of the same length. This is a result of "image forces" on a dislocation near a free surface.

The fact that intentional surface damage does not produce active dislocation sources at the stress levels employed in this investigation is a severe handicap in the investigation of dislocation mobility. It is evident that relatively long lengths of unpinned or weakly pinned dislocation exist in the as-grown crystal, and it is difficult to produce more effective sources by surface damage.

Dislocation mobility

The mobility of basal screw dislocations is of the same order of magnitude as that of basal edge dislocations for the same stress levels at very low strains. This is deduced from the observation that in several pulse tests, pile-ups observed on one of the $(10\bar{1}0)$ surfaces of the test specimen were located on the same slip plane as pile-ups observed on the other $(10\bar{1}0)$ surface within the limit of measurement accuracy. This observation suggests that dislocation loops in zinc expand in a slip plane with the edge and screw dislocation components of the loop traveling at about the same rate. This result is

different from that found for LiF (3) and 3.25% silicon-iron (1) where edge dislocation velocities are much greater than screw velocities at the same stress level.

Figure 9 shows that the direct mobility data for zinc may be appropriately represented as $v = (\tau/\tau_o)^n$ where $\tau_o$ = 5 lb/in.$^2$ which is the stress required to move a dislocation at 1 cm/sec. Mobility data on other materials has been found to fit this same form with different values for n and $\tau_o$. The present results on zinc are the first direct mobility measurements reported on a metal in the so-called "soft" group which includes f.c.c. and h.c.p. metals. The conspicuous difference between basal dislocations in zinc and other materials is the low value of $\tau_o$ which indicates a much lower resistance to dislocation motion.

Thermally activated dislocation motion

Figure 10 shows the dislocation mobility data plotted as log velocity against $\tau - \tau_i$ where $\tau_i$ was taken as 6 lb/in.$^2$ or the lowest stress at which dislocations were observed to move. The slope from Fig. 11 gives B = 1.45 lb/in.$^2$ where B is defined by Eq. 4. The mobility relation as represented by Eq. 4 would be expected if the rate determining mechanism is the thermal activation for a glide dislocation to pass some obstacle in the glide plane. Seeger et al (13) and Friedel (14) have considered this problem and believe that the flow stress for basal glide in hexagonal close-packed crystals is determined by the stress required to overcome the "long-range internal stresses" produced by parallel glide dislocations and by the thermal activation of jogs as basal dislocations glide past forest dislocations threading the glide plane. The strain-rate resulting from thermal activation of jogs is given by Friedel as

$$\dot{\gamma}_p = \rho_m \nu \left(\frac{b}{l}\right)^2 A e^{-\frac{\Delta U - (\tau - \tau_i) bdl}{kT}} \qquad (9)$$

where

$\Delta U$ = energy required to produce the jog
$\tau$ = applied shear stress
$\tau_i$ = long-range internal shear stress
d = separation of extended basal dislocations
l = forest spacing
A = area of slip plane swept over by dislocation after jog is formed
$\nu$ = Debye frequency.

The velocity of a dislocation is then given by

$$v = \nu \frac{b}{l^2} Ae^{-\frac{\Delta U}{kT}} e^{\frac{\tau - \tau_i}{B}} \qquad (10)$$

where

$$B = \frac{kT}{bdl}$$

The forest spacing l for the crystals used in this investigation can be estimated from the etch pit density observed on basal planes ($10^4$ $cm^{-2}$), and is $10^{-2}$ cm . B is then equal to $2.5 \times 10^{-3}$ $lb/in.^2$ if d is taken as 7 b(15). This value of B is considerably lower than the directly determined value of 1.45 $lb/in.^2$. This lack of agreement shows that a model based on the thermal activation of jogs is incapable of explaining the observed dislocation mobility.

One reason the above model is not applicable to zinc can be seen by comparing the terms $\Delta U$ and $(\tau - \tau_i)bdl$ in the exponential term of Eq. 9. For an applied shear stress of 16 $lb/in.^2$, $(\tau - \tau_i)bdl \simeq 20eV$ for the forest spacing observed and a long-range internal stress of about 6 $lb/in.^2$ which is the lowest stress at which basal dislocations were observed to move long distances. $\Delta U$ has been estimated by Friedel (15) to be

$$\Delta U = \frac{Gb^2 d}{30} .$$

$\Delta U$ is then about leV for basal dislocations in zinc. This result means that the applied stress is more than sufficient to supply the jog energy required and thus no assistance from the thermal energy of the lattice is required.

The "activation volume" for a thermally activated process which gives rise to a dislocation velocity described by Eq. 10 is the term bdl. This activation volume is calculated to be $4 \times 10^{-5}$ $cm^3 \simeq 2 \times 10^{18}$ $b^3$ using the experimentally determined value of B. This value of activation volume is large compared to the value expected if the activation event was the formation or motion of kinks on the dislocation lines or the thermally activated motion of dislocations past impurity atoms. Other thermally activated events which give rise to a dislocation velocity described by Eq. 10 can be eliminated as a controlling factor in zinc on the basis of the unreasonably large activation volume observed.

Lattice resistance to dislocation motion

Two possible sources of lattice resistance to dislocation motion in an otherwise perfect lattice have been considered theoretically. Leibfried (16)

was the first to consider the drag on a screw dislocation moving at a constant velocity caused by the scattering of phonons or sound waves and Eshelby (17) has estimated the drag caused by thermoelastic effects. Lothe (18) has recently reviewed and extended the calculations for both effects. Lothe concludes that for metals the thermoelastic effect is negligible and that Leibfried's result for the phonon drag is correct and should be about the same for an edge as well as a screw dislocation. The drag stress due to phonon scatter is given by

$$\tau_d = \frac{1}{10} \epsilon \frac{v}{c_2}$$

where $\epsilon$ is the thermal energy density, v is dislocation velocity and $c_2$ is the velocity of shear waves. Since zinc at room temperature is above the Debye temperature (250° K),

$$\epsilon = \frac{3kT}{b^3}$$

and

$$\tau_d = \frac{0.3\ kTv}{b^3 c_2}$$

where for zinc $b = 2.66 \times 10^{-8}$ cm and $c_2 = 2.31 \times 10^5$ cm/sec.

The phonon drag stress on a dislocation moving at 25 cm/sec in zinc is calculated to be about 1 lb/in.$^2$ which from the present mobility results is a factor of 10 lower than the observed stress required to move a dislocation at this velocity. Seeger (19) has indicated that the damping constant for an edge dislocation should be an order of magnitude greater than that for a screw dislocation which would result in a drag stress of about 10 lb/in.$^2$ for an edge dislocation moving at 25 cm/sec. This is very near the value given by the stress pulse tests for a velocity of 25 cm/sec. The present results suggest that the drag stress could vary as the velocity to the 1/5 power rather than the first power. Considering the uncertainties involved in the theoretical calculations, the possibility that the majority of lattice resistance to moving basal dislocations in Zn may be due to phonon scattering cannot be excluded.

Since the experimental results indicate comparable velocities for edge and screw oriented dislocations, a greater phonon drag stress on edge oriented dislocations would have to be offset by another drag stress acting preferentially on the screw oriented dislocations. Such a drag stress could arise from jogs on the screw oriented segments. The jogs could be formed on the screw oriented segments when cross-slip occurs, and they would not be present on the edge

oriented segments. The absence of broadening of slip lines indicated a relatively small amount of cross-slip in the basal system of zinc as compared to that observed in LiF and many other materials.

Strain-rate sensitivity of the flow stress

Basal dislocations of mixed character are undoubtedly involved in the variable strain rate tests, but the majority of these dislocations must have the same $[\bar{1}2\bar{1}0]$ Burgers vector. It can be shown for this case that the strain-rate equation (Eq. 1) can still be written using the edge dislocation velocity, with an appropriate constant modifying the moving dislocation density term. We may therefore compare the mobilities of edge dislocations observed in the pulse tests with the mobilities indicated in the variable strain-rate tests.

As originally suggested by Guard (7), the dislocation mobility exponent may be deduced from the strain-rate sensitivity of the flow stress providing the number of moving dislocations does not change as a result of the change in strain-rate. The values for $\partial \ln \dot{\gamma}_p / \partial \ln \tau = n'$ determined for zinc crystals are given in Table III. The average value of n' for the two tests is 83. The mobility relation determined by the direct experiments is assumed valid, so that

$$\frac{\partial \ln v}{\partial \ln \tau} = n = 5.$$

Therefore, from Eq. 2

$$\frac{\partial \ln \rho_m}{\partial \ln \tau} = n' - n = 78.$$

This discrepancy between n' and n is large and clearly shows that the number of moving dislocations changes as a result of a strain-rate change.

An alternative model to explain the results found for zinc is proposed where the density of moving dislocations, $\rho_m$, is a function of the difference between the applied shear stress and the flow stress at zero strain-rate, $\tau_f$, or

$$\rho_m = A(\gamma_p)(\tau - \tau_f)^m \qquad (11)$$

$A(\gamma_p)$ is some unknown function of the plastic shear strain and $\tau_f$ may be regarded as the long-range internal stress, $\tau_i$, produced by junction reactions and dislocation pile-ups. It would therefore be a function of $\gamma_p$, that is $\tau_f = \tau_i(\gamma_p)$. The velocity of a moving dislocation is still regarded as a function of $\tau$ because the average stress experienced by a moving dislocation is independent of $\tau_i$ (the internal stress must average to zero along a slip plane). The value of $\tau_i$ used in Eq. 4 is then equivalent to $\tau_i(0)$.

A qualitative picture of the stress difference $\tau - \tau_i$ as a function of

distance along a slip plane is given in Fig. 12. Glide dislocations will be

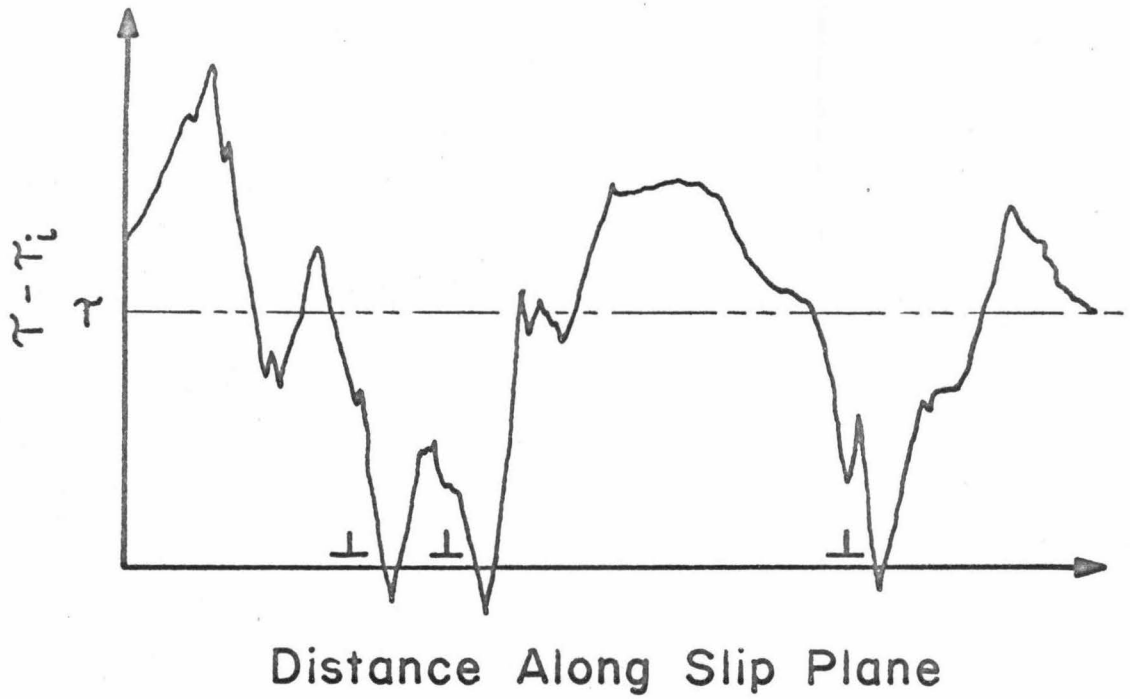


FIG. 12
Variation in Shear Stress Along A Slip Plane

prevented from moving when $\tau - \tau_i$ is negative or equal to zero. This condition is shown for several dislocations. A slight increase in the applied stress will shift the curve upwards allowing some obstructed dislocations to glide. The specific number of dislocations released in this manner would depend on the details of the internal stress variation and, in particular, the distribution of points where $\tau - \tau_i$ goes negative because this stress difference governs whether a dislocation will be released when a given stress change is imposed.

The strain-rate from Eqs. 1, 3, and 11 is now given as

$$\dot{\gamma}_p = A\,(\gamma_p)\,(\tau - \tau_i)^m\,\tau^n$$

and

$$\frac{\partial \ln \dot{\gamma}_p}{\partial \ln \tau} = m\,\frac{\partial \ln(\tau - \tau_i)}{\partial \ln \tau} + n$$

or

$$\frac{\partial \ln \dot{\gamma}_p}{\partial \ln(\tau - \tau_i)} = m + n \frac{\partial \ln \tau}{\partial \ln(\tau - \tau_i)}$$

The experimentally determined values of $\frac{\partial \ln \dot{\gamma}_p}{\partial \ln(\tau - \tau_i)} = m'$ are given in Table III. The term $\frac{\partial \ln \tau}{\partial \ln(\tau - \tau_i)}$ is equal to the ratio m'/n' and is determined experimentally. Therefore, m is given by

$$m = m' \left(1 - \frac{n}{n'}\right)$$

Since n is much less than n', $m \simeq m'$. Table III gives the values of m' determined in the two tests. A value of about 2 was found for both tests. An exponent of m = 2 would be expected if the number of dislocations released per unit length of glide plane were a linear function of the stress difference $\tau - \tau_i$ and if the number of active glide planes were also a linear function of this stress difference.

The model proposed to explain the results for zinc may also apply to other metals of the soft metal group such as copper. Conrad (20) has measured the strain-rate sensitivity of copper single crystals at low temperature and finds that $\partial \ln \dot{\gamma} / \partial \ln \tau$ = 100-200 at 170° K. This result seems clearly unreasonable for a mobility exponent. An alternative interpretation of the results in terms of the newly proposed model is suggested.

More important, many of the conclusions regarding thermally activated mechanisms of dislocation motion which have been drawn from the results of strain-rate change tests are invalid in cases in which the density of moving dislocations changes when the stress changes.

## Conclusions

(i) The mobility of basal edge dislocations in zinc single crystals obeys the relation

$$v = \left(\frac{\tau}{\tau_o}\right)^n$$

for $\tau \geq 6$ lb/in.$^2$, where v is dislocation velocity in cm/sec, n is the mobility exponent and is equal to 5 and $\tau_o$ is 5 lb/in.$^2$. The mobility of screw and edge oriented dislocations appears to be the same. The maximum velocities observed are in the range of 7 to 80 cm/sec for shear stresses between 7 and 12 lb/in.$^2$.

(ii) The mobility results are inconsistent with predictions using

theoretical models which involve the thermally activated motion of glide dislocations past forest dislocations or impurity atoms. The drag stress on a moving dislocation caused by phonon scattering is considered to be a likely velocity limiting process.

(iii) A large difference is observed between the inverse strain-rate sensitivity and the directly determined mobility exponent. A dislocation model is proposed which explains the observed differences. The major part of the strain-rate sensitivity is attributed to changes in the number of moving dislocations which accommodate a change in strain-rate, rather than to the change in dislocation velocity. The proposed dislocation model for the strain-rate sensitivity in zinc may also apply to other h.c.p. and f.c.c. crystals deformed in easy glide, in which large strain-rate changes may be made with very small changes in stress.

## References


1 D. F. Stein and J. F. Low, Jr., J. Appl. Phys., 31 (1960) 362.

2 H. W. Schadler, Acta Met., 12 (1964) 861.

3 W. G. Johnston and J. J. Gilman, J. Appl. Phys., 30 (1959) 129.

4 E. Yu Gutmanas, E. M. Madgornyi and A. V. Stepanov, Fix. Tverd. Tela, 5 (1963) 1021.

5 A. R. Chandhuri, J. R. Patel and L. G. Rubin, J. Appl. Phys., 33 (1962) 2736.

6 M. N. Kabler, Phys. Rev., 131 (1963) 54.

7 R. W. Guard, Acta Met., 9 (1961) 163.

8 W. G. Johnston and D. F. Stein, Acta Met., 11 (1963) 317.

9 A. P. L. Turner, K. H. Adams and T. Vreeland, Jr., Mat. Sci. Eng., 1 (1966) 70.

10 R. C. Brandt, K. H. Adams and T. Vreeland, Jr., J. Appl. Phys., 34 (1963) 587.

11 T. L. Russell, D. S. Wood and D. S. Clark, First Interim Technical Report Under Office of Ordnance Research, Contract No. DA-04-495-ORD-171, California Institute of Technology, 1955.

12 K. H. Adams, Ph.D. Thesis, California Institute of Technology, 1965.

13 A. Seeger, S. Mader and H. Kronmuller, in G. Thomas and J. Washburn (eds.), Electron Microscopy and Strength of Crystals, Interscience, New York, 1963, p. 665.

14 J. Friedel, in G. Thomas and J. Washburn (eds.), Electron Microscopy and Strength of Crystals, Interscience, New York, 1963, 605.

15 J. Friedel, in G. M. Rassweiler and W. L. Grube (eds.), Internal Stresses and Fatigue in Metals, Elsevier, Amsterdam, 1959, 220.

16 G. Leibfried, Z. Physik, 127 (1950) 344.

17 J. D. Eshelby, Proc. Roy. Soc. (London), 197A (1949) 396.

18 J. Lothe, J. Appl. Phys., 33 (1962) 2116.

19 A. Seeger, in J. C. Fisher, W. G. Johnston, R. Thomson and T. Vreeland, Jr. (eds.), Dislocations and Mechanical Properties of Crystals, Wiley, New York, 1957, 447.

20 H. Conrad, Acta Met., 6 (1958) 339.

## Legends To Figures

Fig. 1 Crystallographic Orientation of Test Specimens.

Fig. 2 Prism surface of test specimen prior to pulse testing shown damage produced by two scratches. Line indicates $[\bar{1}2\bar{1}0]$ direction. Magnification X100.

Fig. 3 Tracing of a Typical Pulse Load Record.

Fig. 4 Schematic of Compression Fixture for Rapid Load Machine.

Fig. 5 Schematic of Test Fixture for Strain-Rate Sensitivity Tests.

Fig. 6 Tracing of Oscillograph Record.

Fig. 7 Basal Dislocations Before and After a Pulse of 15.4 $lb/in.^2$, 45 sec Pulse Duration, Specimen 16-2T2, 99.999 per cent Zn Magnification X100.

Fig. 8 Basal Dislocations Before and After a Pulse of 12.2 $lb/in.^2$, $17 \times 10^{-3}$ sec Pulse Duration, Specimen 18-5T1, 99.999 per cent Zn, Magnification X100.

Fig. 9 Basal Dislocation Velocity vs Resolved Shear Stress

Fig. 10 Basal Dislocation Velocity vs $\tau - \tau_i$.

Fig. 11 Schematic of Load vs Time Curve

Fig. 12 Variation in Shear Stress Along A Slip Plane

## Acknowledgments

The authors wish to express their appreciation to the U. S. Atomic Energy Commission for sponsorship of this work under Contract No. AT (04-3)-473. The invaluable assistance of A. P. L. Turner and R. C. Blish in specimen preparation, testing and data analysis is gratefully acknowledged.